Polyoxometalate {W$_{18}$O$_{56}$XO$_6$} Clusters with Embedded Redox-Active Main-Group Templates as Localized Inner-Cluster Radicals**

Laia Vilà-Nadal, Katrin Peuntinger, Christoph Busche, Jun Yan, Daniela Lüders, De-Liang Long, Josep M. Poblet,* Dirk M. Guldi,* and Leroy Cronin*

Polyoxometalates (POMs)[1] are an exceptional family of polynuclear molecular oxide anions usually formed by W, Mo, or V.[2] POMs offer a wide range of structures with diverse physical properties, electronic structures, and applications, such as in catalysis,[3] medicine,[4] materials science,[5] or nanotechnology. Heteropolyoxometalates (HPOMs) are a significant and widely explored subset of POMs. Within this class, the choice of the heteroelement not only determines certain physical properties of the cluster, but increasingly has been found to control the range and connectivity of the building blocks.[6] Amongst the structural diversity of HPOMs architectures, Keggin[7] [M$_{12}$O$_{36}$(XO$_4$)]$^{n-}$ and Wells–Dawson (WD)[8] anions [M$_{18}$O$_{54}$(XO$_4$)$_2$]$^{m-}$ form a basic set of extensively reviewed geometries, which encapsulate tetrahedral heteroanions such as [SO$_4$]$^{2-}$ and [PO$_4$]$^{3-}$. In general, POMs exhibit significant stability for both the oxidized and one-electron-reduced form,[9] and the electrochemistry of HPOMs has been extensively studied.[10] In this respect, in an effort to tune the redox properties of POMs, we have been able to engineer clusters that incorporate redox-active anions and expand the classic WD family. These new non-classical Dawson clusters, with the general formula [H$_n$M$_{18}$O$_{56}$(XO$_6$)]$^{m-}$ (X = W^{VI}, Te^{VI}, I^{VII}), embed one octahedral or trigonal prismatic template within the cluster shell.[11] Electrochemical studies demonstrated that classic WD anions are reduced through multiple steps of two electrons (at pH 7) without degradation of the heteropoly structure.

The process generates reduced species, known as heteropoly blues owing to their characteristic blue color,[12] with the WD structures having two types of metal sites: cap and the belt (Figure 1). In the classic WD structures, these "blue"
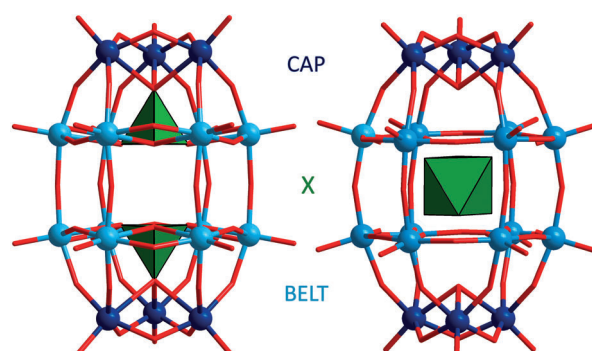

Figure 1. Structural representation of the two polyoxometalate (POM) geometries studied herein. Left: Wells–Dawson cluster with two tetrahedral guests [M$_{18}$O$_{54}$(XO$_4$)$_2$]$^{m-}$ (X = P^V, S^{IV}, As^V, ...). Right: non-conventional Wells–Dawson cluster with one octahedral guest [H$_n$M$_{18}$O$_{56}$(XO$_6$)]$^{m-}$ (X = I^{VII}, Te^{VI}, W^{VI}). The frameworks {W$_{18}$O$_{54}$} and {W$_{18}$O$_{56}$} are shown as ball (W), stick (O), and the heteroatoms in a polyhedral representation. O red, W blue, X green. The WD cluster has two different metal positions, six polar (or cap; dark blue) and twelve equatorial (or belt; light blue) sites.

electrons are delocalized only over the belt metal atoms.[13] NMR spectroscopy experiments on the reduced species show that electron delocalization is restricted to the two hexagonal belts and are completely spin-paired at room temperature.[14]

Herein, we present the first Dawson-like {W$_{18}$O$_{56}$XO$_6$} clusters (X = I or Te) with localized redox active inner-cluster templates, and we show that these moieties can adopt different oxidation states; for example, I$^{VII/VI}$ or Te$^{VI/V}$, respectively. To investigate this in detail, we used cyclic voltammetry, UV and EPR spectroscopy combined with experimental comparison to a control, non-heteroatom embedded Dawson-like cluster. We also evaluated the electronic structure of both the oxidized and reduced forms of the clusters using DFT based upon X-ray data of the oxidized forms.[11] As a built-in control we used a Dawson-like tungstate cage {W$_{18}$O$_{56}$}, where the template is [WO$_6$]$^{6-}$ (TPA$_6$[H$_4$W$_{18}$O$_{56}$(WO$_6$)], abbreviated as WW$_{18}$; TPA = tetrapropylammonium),[15] as a reference system to compare directly with the [TeO$_6$]$^{6-}$ (γ*-TPA$_7$[H$_3$W$_{18}$O$_{56}$(TeO$_6$)]/γ*-TeW$_{18}$)[11d] and [IO$_6$]$^{5-}$ (β*-TPA$_6$[H$_3$W$_{18}$O$_{56}$(IO$_6$)]/β*-

[*] Dr. L. Vilà-Nadal,[+] Dr. C. Busche,[+] Dr. J. Yan, Dr. D.-L. Long, Prof. Dr. L. Cronin
WestCHEM, School of Chemistry, The University of Glasgow
Glasgow G12 8QQ (UK)
E-mail: Lee.Cronin@glasgow.ac.uk
Homepage: http://www.croninlab.com

K. Peuntinger,[+] D. Lüders, Prof. Dr. D. M. Guldi
Department of Chemistry and Pharmacy and Interdisciplinary Center for Molecular Materials
Friedrich-Alexander-University Erlangen-Nürnberg
Egerlandstrasse 3, 91058 Erlangen (Germany)
E-mail: dirk.guldi@chemie.uni-erlangen.de

Prof. Dr. J. M. Poblet
Departament de Química Física i Inorgànica
Universitat Rovira i Virgili, c/Marcel·lí Domingo s/n
43007 Tarragona (Spain)
E-mail: josepmaria.poblet@urv.cat

[+] These authors contributed equally to this work.

Angew. Chem. Int. Ed. **2013**, *52*, 9695–9699

© 2013 Wiley-VCH Verlag GmbH & Co. KGaA, Weinheim

WILEY ONLINE LIBRARY

9695

IW$_{18}$)[11c] templated WD structures. In our study we present the redox behavior of non-classical WD POMs. Not only do we detect that γ*-TeW$_{18}$ and β*-IW$_{18}$, initially exhibit a localized one-electron process whereby the central hetero-atom is reduced Te$^{VI \to V}$, I$^{VII \to VI}$, but we also find that reduction at more negative potentials also reduces the tungsten framework, resulting in a mixture between a localized and delocalized electron-containing species.

The whole redox process is completely controllable and reversible, and the reduction of specific sites in POMs is well-known, for example, in the case of vanadium-substituted POMs such as $[XV^VM_{11}O_{40}]^{4-}$ (X = P, As; M = W, Mo), which exhibit a V^V to V^{IV} reduction.[16] However, to the best of our knowledge, this is the first time that a reduced POM with a localized electron located on a main-group heteroatom has been described, and as such these compounds show a new type of localized inner-cluster radical.

Cyclic voltammetry studies on $[H_nM_{18}O_{56}(XO_6)]^{m-}$ (X = W, Te, I) using a glassy carbon electrode in acetonitrile showed a series of reversible one-electron redox processes (potentials are summarized in Table 1, Figure 2, and the

Supporting Information, Figures S1–S3). Assignment of a one-electron reduction process is supported by bulk electrolysis (see the Supporting Information). The first reduction of WW$_{18}$ showed a visually noticeable optical contrast (transparent to blue), which is due to the W^{IV} to W^V reduction process, and it should be noted that this behavior was not observed for the one-electron-reduced species of γ*-TeW$_{18}$ and β*-IW$_{18}$. To gain further understanding of the reduction process, we have performed spectroelectrochemical measurements. The UV/Vis absorption spectrum of reduced and non-reduced clusters is shown in Figure 2. The three two-electron reduced clusters show a broad absorption at about 700 nm, which is characteristic for reduced POMs.[17] These data suggest that for the singly reduced $\{W_{18}O_{56}XO_6\}$, when X = I or Te, the electron is localized on the template $\{XO_6\}$.

For the initial one-electron-transfer step we performed bulk reductive electrolysis, and the EPR spectra obtained after bulk electrolysis at the first reduction potential are indicative for Te^V and I^{VI}. The one- and two-electron processes for compounds WW$_{18}$, γ*-TeW$_{18}$, and β*-IW$_{18}$ are described in Equations (1) to (6):
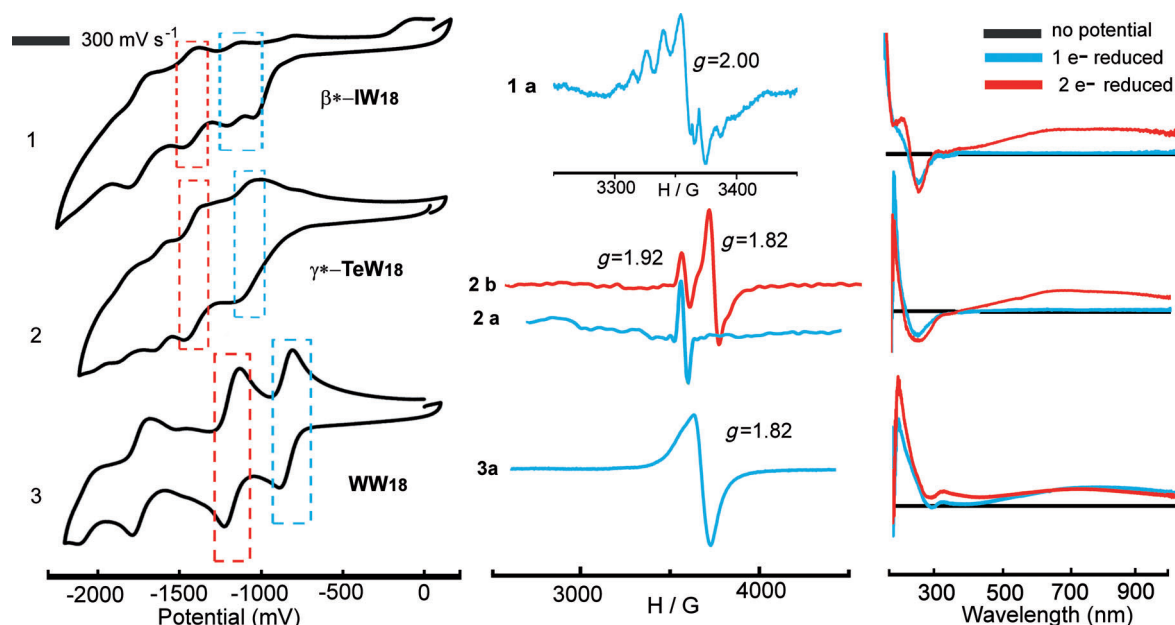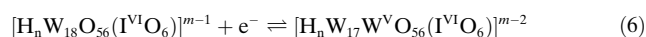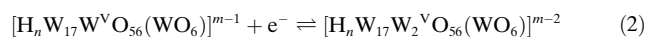
Table 1: Summary of the reversible potentials for the reduction of $[H_nM_{18}O_{56}(XO_6)]^{m-}$ (X = W, Te, I) at a glassy carbon electrode in acetonitrile.[a]

	E^0 [mV] vs. Fc/Fc$^+$		
m	6-/7-	7-/8-	8-/9-
$[H_4W_{18}O_{56}(WO_6)]^m$	−596	−933	−1497
m	7-/8-	8-/9-	9-/10-
$[H_3W_{18}O_{56}(TeO_6)]^m$	−918	−1255	−1448
m	6-/7-	7-/8-	8-/9-
$[H_3W_{18}O_{56}(IO_6)]^m$	−916	−1179	−1496

[a] See the Supporting Information for further details.

$$[H_nW_{18}O_{56}(WO_6)]^{m-} + e^- \rightleftharpoons [H_nW_{17}W^VO_{56}(WO_6)]^{m-1} \tag{1}$$

$$[H_nW_{17}W^VO_{56}(WO_6)]^{m-1} + e^- \rightleftharpoons [H_nW_{17}W_2^VO_{56}(WO_6)]^{m-2} \tag{2}$$

$$[H_nW_{18}O_{56}(TeO_6)]^{m-} + e^- \rightleftharpoons [H_nW_{18}O_{56}(Te^VO_6)]^{m-1} \tag{3}$$

$$[H_nW_{18}O_{56}(Te^VO_6)]^{m-1} + e^- \rightleftharpoons [H_nW_{17}W^VO_{56}(Te^VO_6)]^{m-2} \tag{4}$$

$$[H_nW_{18}O_{56}(IO_6)]^{m-} + e^- \rightleftharpoons [H_nW_{18}O_{56}(I^{VI}O_6)]^{m-1} \tag{5}$$

$$[H_nW_{18}O_{56}(I^{VI}O_6)]^{m-1} + e^- \rightleftharpoons [H_nW_{17}W^VO_{56}(I^{VI}O_6)]^{m-2} \tag{6}$$

Figure 2. Left: Selected cyclic voltammograms at 300 mV s^{-1} scan rate: 1) β*-IW$_{18}$; 2) γ*-TeW$_{18}$; 3) WW$_{18}$. The first reduction is highlighted in blue (-----) and the second reduction in red (-----). Center: EPR spectra of acetonitrile solutions at 100 K: 1 a) one-electron-reduced β*-IW$_{18}$, showing the ^{127}I hyperfine structure. 2 a) one-electron-reduced γ*-TeW$_{18}$ (blue); 2 b) two-electron-reduced γ*-TeW$_{18}$ (red); 3 a) one-electron-reduced WW$_{18}$ (blue). Right: Spectroelectrochemistry: Delta absorption spectra (ΔOD): 1) β*-IW$_{18}$; 2) γ*-TeW$_{18}$; and 3) WW$_{18}$ in acetonitrile under argon.

The EPR spectra after one-electron reduction of WW$_{18}$, γ*-TeW$_{18}$, and β*-IW$_{18}$ are shown in Figure 2 and the Supporting Information. In the case of WW$_{18}$, we observe a broad signal with a g value of 1.82, this value is within the range found for axial oxo complexes of tungsten(V).[18] In contrast, for clusters γ*-TeW$_{18}$ and β*-IW$_{18}$, we observed a sharp signal with a g value 1.92, while the solution stayed colorless, indicating a localized

Figure 3. Diagram of the molecular orbitals of α-[W$_{18}$O$_{54}$(PO$_4$)$_2$]$^{6-}$ (α-P$_2$W$_{18}$), α- and γ*-[W$_{18}$O$_{56}$(WO$_6$)]$^{10-}$ (α-,γ*-WW$_{18}$), γ*-[W$_{18}$O$_{56}$(TeO$_6$)]$^{10-}$ (γ*-TeW$_{18}$), and β*-[W$_{18}$O$_{56}$(IO$_6$)]$^{9-}$ (β*-IW$_{18}$). Cap and belt indicates the localization of each MO in the POM geometry.

electron on the template of the cluster, forming a non-mixed-valent reduced species. In the case of one-electron-reduced β*-IW$_{18}$, we observed hyperfine splitting arising from the ^{127}I nuclei, which is another clear indicator for the heteroatom-localized electron. After re-oxidizing the samples, the signals disappeared, and the samples could once again be reduced, giving the same behavior, and this serves as clear evidence of a fully reversible process. When transferring two electrons by bulk electrolysis, no changes were obtained for the reference compound WW$_{18}$. For cluster γ*-TeW$_{18}$ and β*-IW$_{18}$, however, we received a set of two signals, one indicating a delocalized electron over the shell (g value 1.82), characterized also by the blue color of the solution, and the other exhibiting the localized electron on the template (g value 1.92; see the Supporting Information).

Guided by the experimental results we have also conducted density functional theory (DFT) calculations on the clusters, as the DFT formalism is a very useful method to understand electronic and magnetic properties of POMs.[19] The conventional Wells–Dawson cluster α-[W$_{18}$O$_{54}$(PO$_4$)$_2$]$^{6-}$ α-P$_2$W$_{18}$ is one of the most reviewed tungstophosphates since the resolution of its structure more than 50 years ago,[20] and it is taken here as benchmark for the calculations. Previous studies have helped to rationalize the isomerism and the redox properties of the classic Wells–Dawson heteropolyanions.[21] In one of our more recent studies, we determined that the stability of isomers α*, β*, and γ* in the non-classical structures can be easily rationalized from the analysis of the frontier orbitals;[22] herein we have applied the same theoretical approach to understand their electrochemical behavior.

In general terms, the electronic structure of a fully oxidized POM is quite simple: doubly occupied orbitals (HOMO) are formally delocalized over the oxo ligands and are perfectly separated from the unoccupied set of d-metal orbitals (LUMO)[23] (see the Experimental Section and Supporting Information for more details). The relative energies of the lowest unoccupied orbitals in the fully oxidized classic WD, [W$_{18}$O$_{54}$(PO$_4$)$_2$]$^{6-}$, and the four non-classic Wells-Dawson structures, [H$_n$M$_{18}$O$_{56}$(XO$_6$)]$^{m-}$ (X = W, Te, and I) are compared in Figure 3. When the central heteroatom is tungsten, the LUMO and LUMO+1 are mainly delocalized over the belt metals, as occurs in the classic α-P$_2$W$_{18}$ structure. Consequently, the first reduction of WW$_{18}$

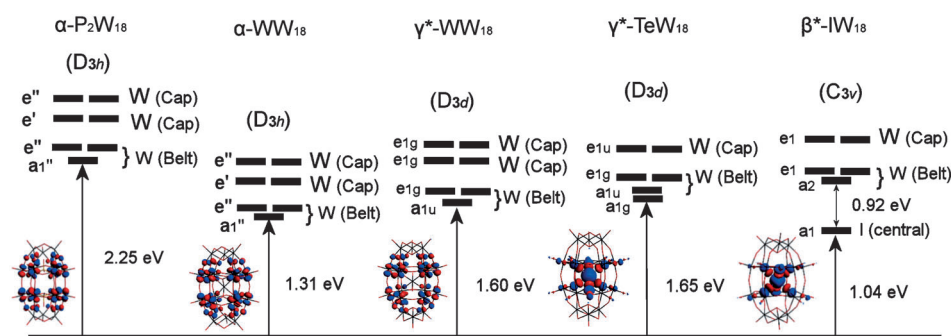would take place at the equatorial region. Inclusion of Te and I as central atoms modifies the energy and composition of the lowest unoccupied orbitals. This modification of the traditional distribution of the LUMOs is due to the greater electron affinities of Te and I. Thus in the case of γ*-TeW$_{18}$ and β*-IW$_{18}$, the LUMO is mainly localized at the central heteroatom, and therefore the first reduction takes place at the tellurium and iodine centers.

According to the molecular orbital diagram in Figure 3, the reduction on the belt tungsten atoms would require about 1 eV more than the reduction of the more electronegative iodine center. In this kind of system, orbital energy differences permit a good estimation of the reduction energy differences.[23a] This phenomenon is comparable to the mixed metal heteropolyanions, for instance the trisubstituted [P$_2$W$_{15}$V$_3$O$_{62}$]$^{9-}$ Wells–Dawson anion, which is preferably reduced in the vanadium polar sites.[23]

A simple analysis of the frontier orbitals of the fully oxidized molecules helped us to rationalize the first two examples of non-blue, non-mixed-valent singly reduced clusters. Calculations performed on the reduced structures confirmed our hypothesis (Supporting Information, Tables S1, S2). The ground state for the singly reduced WW$_{18}$ has nearly 80% of the spin density delocalized over the belt atoms, whereas γ*-TeW$_{18}$ and β*-IW$_{18}$ singly reduced clusters have the spin density mainly localized at the six oxygen atoms of the central {XO$_6$} moiety. The spin density shows some polarization, with 0.12 α electrons localized over the Te and 0.72 β electrons delocalized over the oxygen atoms. A similar situation is observed when the central unit is {IO$_6$}, namely 0.12 α and 0.73 β electrons (Supporting Information, Tables S3, S4 and Figure S11). Spin polarization is a mechanism related to the minimization of Coulomb (J_{ij}) and exchange (K_{ij}) integrals (see Ref. [24] for a wide discussion in MX$_6$ systems). For the WW$_{18}$ doubly reduced clusters, the spin polarization is also mainly located at the belt. In the case of the doubly reduced γ*-TeW$_{18}$ and β*-IW$_{18}$ clusters, the spin density is delocalized over the belt and the central {XO$_6$} moiety. Our experimental data is in agreement with these results and demonstrates that the first reduction of γ*-TeW$_{18}$ and β*-IW$_{18}$ occurs on the central {XO$_6$} unit. For further information regarding calculations on the reduced structures, see the Supporting Information, Tables S1–S4.

In summary, we have been able to show, for the first time, that it is possible to reduce a heteropoly anion to give a localized electron on the inner heteroatom main-group template; in this case involving the Dawson-like cluster when X = I or Te. This unusual behavior differs fundamentally from the classic reduced POMs with the electron delocalized over the metal shell. Thus, these investigations indicate that it may be possible to configure this unique class of POMs as a new type of inner-sphere electron transfer device/reagent and even for new applications in electronic devices, which is currently being explored in our laboratory. In future work, we will try and engineer a classical Keggin structure with a redox active main-group heteroanions, as we believe such clusters will also show novel electronic properties. Finally, we will also investigate how the embedded inner-cluster heteroatom becomes reduced, including if the idea that the incoming reducing electron is initially transiently "trapped" by the shell before being conducted to the heteroatom center through bonds or space.[27]

Experimental Section

All of the solvents were of spectroscopic grade and used without any further purification.

Electrochemical data were obtained by cyclic voltammetry using FRA 2 Autolab Typ III Potentiostat/Galvanostat (with impedance unit) (METROM) with a glassy carbon working electrode, Pt wire counter electrode, and Ag wire pseudo reference electrode (see the Supporting Information) in the usual three-electrode setup. The measurements were carried out in anhydrous and argon saturated acetonitrile. Tetrabutylammonium hexafluorophosphate was used as electrolyte (0.1M). The redox potential of ferrocenium/ferrocene was found to be at 0.4 V ($E_{(Fc^+/Fc)} = 0.40$ V). Bulk electrolysis experiments were carried out using a CHI600D computer-controlled electro-analytical system in the potentiostate mode with a carbon-felt working electrode, Pt wire counter electrode, and Ag/AgCl reference electrode. All potentials are referenced to ferrocenium/ferrocene.

Spectroelectrochemical experiments were carried out using a METROHM PGSTAT 101 and a SPECORD S600 Analytic Jena spectrophotometer. The measurements were performed in a quartz glass cuvette, optical path length 1.0 mm, containing a three-electrode arrangement: a light-transparent platinum gauze as a working electrode, a Ag/AgNO$_3$ reference electrode, and a platinum plate as counter electrode. Tetrabutylammonium hexafluorophosphate (0.1M) was used as supporting electrolyte in acetonitrile under an argon atmosphere. All potentials are referenced to ferrocenium/ferrocene.

X-Band EPR spectra were recorded on a Bruker Elexsys E500 spectrometer with a cylindrical TE$_{011}$ cavity as approximately 1×10^{-4} M frozen acetonitrile solution at $T = 100$ K.

Calculations were carried out using DFT with the ADF 2008 program.[25] The exchange-correlation functionals of Becke and Perdew were used.[26] Relativistic corrections were included by means of the ZORA formalism. Triple-ζ polarization basis sets were employed to describe the valence electrons of W, O, P, Te, and I. All of the structures were optimized in the presence of a continuous model solvent by means of the conductor-like screening model (COSMO). See the Supporting Information for more details on the computational settings.

[1] M. T. Pope, *Heteropoly and Isopoly Oxometalates*, Springer, New York, **1983**.

[2] a) D.-L. Long, E. Burkholder, L. Cronin, *Chem. Soc. Rev.* **2007**, *36*, 105–121; b) D.-L. Long, H. Abbas, P. Kögerler, L. Cronin, *J. Am. Chem. Soc.* **2004**, *126*, 13880–13881.

[3] J. T. Rhule, W. A. Neiwert, K. I. Hardcastle, B. T. Do, C. L. Hill, *J. Am. Chem. Soc.* **2001**, *123*, 12101–12102.

[4] J. T. Rhule, C. L. Hill, D. A. Judd, R. F. Schinazi, *Chem. Rev.* **1998**, *98*, 327–358.

[5] a) D.-L. Long, L. Cronin, *Chem. Eur. J.* **2006**, *12*, 3698–3706; b) Y.-F. Song, N. McMillan, D.-L. Long, J. Thiel, Y. Ding, H. Chen, N. Gadegaard, L. Cronin, *Chem. Eur. J.* **2008**, *14*, 2349–2354; c) Y.-F. Song, D.-L. Long, L. Cronin, *Angew. Chem.* **2007**, *119*, 3974–3978; *Angew. Chem. Int. Ed.* **2007**, *46*, 3900–3904; d) Y.-F. Song, H. Abbas, C. Ritchie, N. McMillian, D.-L. Long, N. Gadegaard, L. Cronin, *J. Mater. Chem.* **2007**, *17*, 1903–1908.

[6] J. Yan, D.-L. Long, L. Cronin, *Angew. Chem.* **2010**, *122*, 4211–4214; *Angew. Chem. Int. Ed.* **2010**, *49*, 4117–4120.

[7] J. F. Keggin, *Nature* **1933**, *131*, 908–909.

[8] a) B. Dawson, *Acta Crystallogr. Sect. B* **1953**, *6*, 113–126; b) R. Strandberg, *Acta Chem. Scand. Ser. A* **1975**, *29*, 350–358.

[9] J. Nambu, T. Ueda, S.-X. Guo, J. F. Boas, A. M. Bond, *Dalton Trans.* **2010**, *39*, 7364–7373.

[10] a) M. T. Pope, E. Papaconstantinou, *Inorg. Chem.* **1967**, *6*, 1147–1152; b) E. Papaconstantinou, M. T. Pope, *Inorg. Chem.* **1970**, *9*, 667–669; c) M. Sadakane, E. Steckhan, *Chem. Rev.* **1998**, *98*, 219–237; d) B. Keita, L. Nadjo, *J. Mol. Catal. A* **2007**, *262*, 190–215.

[11] a) D.-L. Long, P. Kögerler, A. D. C. Parenty, J. Fielden, L. Cronin, *Angew. Chem.* **2006**, *118*, 4916–4921; *Angew. Chem. Int. Ed.* **2006**, *45*, 4798–4803; b) C. Ritchie, E. M. Burkholder, D.-L. Long, D. Adam, P. Kögerler, L. Cronin, *Chem. Commun.* **2007**, 468–470; c) D.-L. Long, Y. F. Song, E. F. Wilson, P. Kögerler, S. X. Guo, A. M. Bond, J. S. J. Hargreaves, L. Cronin, *Angew. Chem.* **2008**, *120*, 4456–4459; *Angew. Chem. Int. Ed.* **2008**, *47*, 4384–4387; d) J. Yan, D.-L. Long, E. F. Wilson, L. Cronin, *Angew. Chem.* **2009**, *121*, 4440–4444; *Angew. Chem. Int. Ed.* **2009**, *48*, 4376–4380.

[12] a) P. Day, N. S. Hush, R. J. H. Clark, *Philos. Trans. R. Soc. London Ser. A* **2008**, *366*, 5–14; b) L. E. Briand, G. T. Baronetti, H. J. Thomas, *Appl. Catal. A* **2003**, *256*, 37–50.

[13] M. T. Pope in *Polyoxometalate Molecular Science* (Eds.: J. J. Borrás-Almenar, E. Coronado, A. Müller, M. T. Pope), *NATO Science Series*, Kluwer Academic Publishers, Dordrecht, **2001**, p. 21.

[14] a) J. J. Borrás-Almenar, J. M. Clemente, E. Coronado, B. S. Tsukerblat, *Chem. Phys.* **1995**, *195*, 17–28; b) M. Kozik, C. F. Hammer, L. C. W. Baker, *J. Am. Chem. Soc.* **1986**, *108*, 2748–2749; c) M. Kozik, N. Casañ-Pastor, C. F. Hammer, L. C. W. Baker, *J. Am. Chem. Soc.* **1988**, *110*, 7697–7701; d) H. Duclusaud, S. A. Borshch, *J. Am. Chem. Soc.* **2001**, *123*, 2825–2829.

[15] Mixture of both isomers α and γ*; see Ref. [11a] for more details.

[16] S. P. Harmalker, M. A. Leparulo, M. T. Pope, *J. Am. Chem. Soc.* **1983**, *105*, 4286–4292.

[17] E. Papaconstantinou, *Chem. Soc. Rev.* **1989**, *18*, 1–31.

[18] a) G. M. Varga, Jr., E. Papaconstantinou, M. T. Pope, *Inorg. Chem.* **1970**, *9*, 662–667; b) R. A. Prados, M. T. Pope, *Inorg. Chem.* **1976**, *15*, 2547–2553.

[19] a) J. M. Poblet, X. López, C. Bo, *Chem. Soc. Rev.* **2003**, *32*, 297–308; b) A. J. Bridgeman, G. Cavigliasso, *J. Phys. Chem. A* **2003**, *107*, 6613–6621; c) X. López, J. A. Fernández, J. M. Poblet, *Dalton Trans.* **2006**, 1162–1167; d) X. López, J. J. Carbó, C. Bo, J. M. Poblet, *Chem. Soc. Rev.* **2012**, *41*, 7537–7571.

[20] a) A. F. Wells in *Structural Inorganic Chemistry*, Oxford University Press, Oxford, 1st ed., **1945**, p. 344.

[21] a) X. López, C. Bo, J. M. Poblet, J. P. Sarasa, *Inorg. Chem.* **2003**, *42*, 2634 – 2638; b) F.-Q. Zhang, W. Guan, L.-K. Yan, Y.-T. Zhang, M.-T. Xu, E. Hayfron-Benjamin, Z.-M. Su, *Inorg. Chem.* **2011**, *50*, 4967 – 4977.

[22] L. Vilà-Nadal, S. G. Mitchell, D. L. Long, A. Rodríguez-Fortea, X. López, J. M. Poblet, L. Cronin, *Dalton Trans.* **2012**, *41*, 2264 – 2271.

[23] a) X. López, C. Bo, J. M. Poblet, *J. Am. Chem. Soc.* **2002**, *124*, 12574 – 12582; b) J. M. Maestre, X. López, C. Bo, J. M. Poblet, N. Casañ-Pastor, *J. Am. Chem. Soc.* **2001**, *123*, 3749 – 3758.

[24] a) E. Ruiz, J. Cirera, S. Alvarez, *Coord. Chem. Rev.* **2005**, *249*, 2649 – 2660; b) J. Cano, E. Ruiz, S. Alvarez, M. Verdaguer, *Comments Inorg. Chem.* **1998**, *20*, 27 – 56.

[25] a) ADF 2008.01, Department of Theoretical Chemistry. Vrije Universiteit, Amsterdam; b) G. T. te Velde, F. M. Bickelhaupt, E. J. Baerends, C. F. Guerra, S. J. A. Van Gisbergen, J. G. Snijders, T. Ziegler, *J. Comput. Chem.* **2001**, *22*, 931 – 967.

[26] a) A. D. Becke, *Phys. Rev. A* **1988**, *38*, 3098 – 3100; b) J. P. Perdew, *Phys. Rev. B* **1986**, *33*, 8822 – 8824; c) C. Lee, W. Yang, R. Parr, *Phys. Rev. B* **1988**, *32*, 785 – 789.

[27] P. P. Edwards, H. B. Gray, M. T. J. Lodge, R. J. P. Williams, *Angew. Chem.* **2008**, *120*, 6860 – 6868; *Angew. Chem. Int. Ed.* **2008**, *47*, 6758 – 6765.